

Trapping of microparticles in the near field of an ultrasonic transducer

Tobias Lilliehorn^{a,*}, Urban Simu^a, Mikael Nilsson^b, Monica Almqvist^b,
Tadeusz Stepinski^a, Thomas Laurell^b, Johan Nilsson^b, Stefan Johansson^a

^a Department of Engineering Sciences, Uppsala University, Box 534, SE-75121 Uppsala, Sweden

^b Department of Electrical Measurement Technology, Lund Institute of Technology, Lund, Sweden

Accepted 4 November 2004

Available online 23 November 2004

Abstract

We are investigating means of handling microparticles in microfluidic systems, in particular localized acoustic trapping of microparticles in a flow-through device. Standing ultrasonic waves were generated across a microfluidic channel by ultrasonic microtransducers integrated in one of the channel walls. Particles in a fluid passing a transducer were drawn to pressure minima in the acoustic field, thereby being trapped and confined at the lateral position of the transducer. The spatial distribution of trapped particles was evaluated and compared with calculated acoustic intensity distributions. The particle trapping was found to be strongly affected by near field pressure variations due to diffraction effects associated with the finite sized transducer element. Since laterally confining radiation forces are proportional to gradients in the acoustic energy density, these near field pressure variations may be used to get strong trapping forces, thus increasing the lateral trapping efficiency of the device. In the experiments, particles were successfully trapped in linear fluid flow rates up to 1 mm/s. It is anticipated that acoustic trapping using integrated transducers can be exploited in miniaturised total chemical analysis systems (μ TAS), where e.g. microbeads with immobilised antibodies can be trapped in arrays and subjected to minute amounts of sample followed by a reaction, detected using fluorescence.

© 2004 Elsevier B.V. All rights reserved.

Keywords: Ultrasound; Near field; Trap; Piezoelectric; PZT; Microfluidic; Particles

1. Introduction

Particle handling in miniaturised total chemical analysis systems (μ TAS) has begun to receive attention due to the prospect of using particles or beads with a large surface area and tailored surface chemistry for performing bioassays. Physical barriers may be utilized to trap particles during reaction and analysis [1–3] but to allow for a more flexible trapping of particles in biospecific arrays in a fluidic chamber, an alternative trapping technique is desired. In this paper we thus evaluate

acoustically controlled trapping of microparticles within a microchannel using integrated ultrasonic microtransducers. The integration of microtransducers is expected to create opportunities for novel applications that are not possible to reach with conventional macro scale components, such as arrays of distributed and individually addressable particle trapping positions in microfluidic systems.

Particles subjected to acoustic waves are influenced by acoustic radiation forces, which are particularly strong in standing wave fields [4]. The forces can be divided into axial and transverse components of the primary radiation force, and secondary particle–particle interactions due to scattering of incident waves [5]. The acoustic properties of the particulate material as

* Corresponding author. Tel.: +46 18 471 7236; fax: +46 18 471 3572.

E-mail address: tobias.lilliehorn@angstrom.uu.se (T. Lilliehorn).

compared to the surrounding medium determine whether the primary radiation force is directed towards the pressure nodes or antinodes in a standing wave. Typical polymer particles gather at pressure nodes when subjected to an acoustic standing wave in water. The magnitude of the radiation force is proportional to the acoustic frequency [5] and for particle manipulation it is therefore advantageous to increase the frequency to the ultrasonic region. Consequently ultrasonics has successfully been used to manipulate particles or biological material, e.g. as acoustic tweezers [6] and for particle separation from continuous fluid flow in macro- [7] and microscale devices [8]. Two-dimensional trapping and manipulation of microorganisms has been performed using orthogonal standing waves [9]. Sizeselective ultrasonic trapping of microbeads in capillaries has also been investigated [10,11] in order to allow separation of immunocomplexes for trace-amount protein detection. Other bio-related applications making use of acoustic forces include separation of fat from blood during cardiovascular surgery [12] and the retention of mammalian cells in cell culture fermentations [13]. None of these papers however address the issue of trapping particles in microfluidic systems with the prospect of performing bioassays in a bead-based array format.

When performing bead-based bioanalytic assays within a trapping device, it is desirable to keep the particles away from the interior surfaces during trapping. This is thought to minimise carry over between assays when new beads are introduced in the trap. By designing an acoustic resonator to position a pressure node within the fluid, particles can be collected within this nodal plane. The acoustic field in resonators for ultrasonic particle manipulation has been investigated and modelled previously [7,14–16]. The modelling includes the thickness and acoustic properties of the resonator layers (transducer, matching, fluid and reflector) but is restricted to the one-dimensional case with propagation of the sound wave in one direction only.

In this paper we present a novel microfluidic device based on a microresonator that employs integrated microtransducers for particle trapping. To improve electrical matching of the piezoceramic microtransducers to the driving electronics [17], the transducers are constructed with integrated multilayer sandwich electrodes. Considering that the lateral dimensions of the transducers are in the same order of magnitude as the acoustic wavelength in the resonator, three-dimensional effects such as near field pressure variations [18] are expected. This has previously been noted to allow stable off-axis positioning of specimens in a macroscale acoustic levitator radiating in air [19]. The possibility to use near field effects for lateral particle trapping in a microfluidic device is evaluated experimentally and the results compared with calculations of the three-dimensional acoustic field within the resonator.

2. Experimental

2.1. Design

The design of the microresonator is shown schematically in Fig. 1. The $\lambda/2$ wavelength fluid layer (b), conducting the particle suspension was enclosed by an air-backed miniature transducer (c) with a thickness of $\lambda/2$ and a reflector (a) with a thickness of $(2n + 1)\lambda/4$. The transducer was thus positioned in direct contact with the fluid.

2.2. Transducer manufacturing

The lead zirconate titanate (PZT) transducers were batch-wise fabricated in the green state using multilayer wet building of PZT¹ slurry and computer numerically controlled (CNC) machining of screen-printed platinum electrodes according to previously published work [20]. Transducer elements were manufactured with green dimensions 1.0 mm square. The elements were composed of a total of three active PZT layers sandwiched between inactive layers. After sintering, external Ag electrodes were applied for electrical connection to the internal electrodes. The sintered transducer elements were measured to be $0.80 \times 0.83 \text{ mm}^2$ with a layer thickness of active layers being $36 \mu\text{m}$. The transducer elements were thinned by polishing, tuning the element thickness resonance to near 10.6 MHz. Finally, the PZT material was polarised by applying 50 V over the external electrodes for 2 min at room temperature.

2.3. Device manufacturing and assembly

Printed circuit boards (PCBs), $26 \times 26 \text{ mm}^2$, supplying electrical connection to the transducer elements were CNC machined from copper–epoxy laminate. Holes were drilled through the boards for fluidic connections and in the positions of the transducer elements for air backing. On each board, three transducer elements covering the drilled holes were mounted and electrically connected using conductive Ag epoxy² as shown in Fig. 2. Epoxy³ was thereafter cast over the boards, hardened and polished down to the upper surface of the transducer elements. Silicon rubber connectors were attached to the backside of the PCBs for fluidic connection (inlets and outlets) via the drilled holes and through the epoxy layer.

Channels were microfabricated using SU-8⁴ thick photoresist on 1.55 mm thick soda-lime glass substrates. The channels were designed to be 1.0 mm wide and to fit

¹ EDO EC-76, EDO Ceramics, USA.

² Circuit Works 2400, Chemtronics, USA.

³ Epotek 353ND, Epoxy Technology, USA.

⁴ SU8-50, MicroChem, USA.

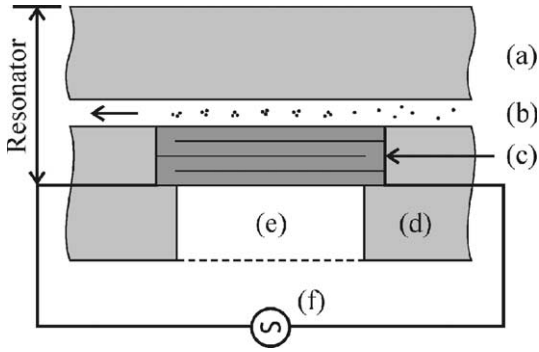


Fig. 1. Resonator build-up showing reflector (a), fluid layer conducting particle suspension (b), multilayer transducer element (c) baffle (d) and air backing (e). The transducer was driven by a function generator (f) to generate ultrasonic waves. An arrow indicates the flow direction within the fluid layer.

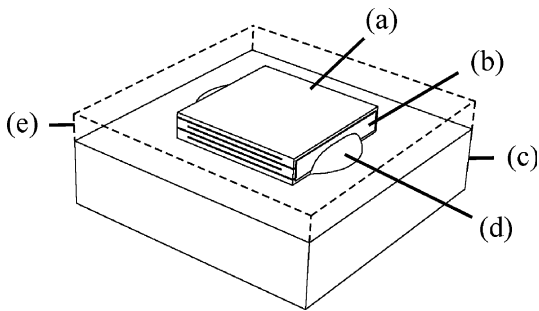


Fig. 2. Multilayer transducer element (a) with the external Ag electrodes (b) connected to the circuitry on the PCB (c) with conductive Ag epoxy (d). The board was covered with epoxy (e).

the fluidic connections on the PCBs with one inlet for particle suspension, one for water and a common outlet, as shown in Fig. 3. Excess fluid connections, forming crosses at the transducer positions, were added for future use and to avoid lateral channel resonances. SU-8 was applied by spin coating, forming an approximately 80 μm thick layer that was patterned using photolithographic techniques [21]. The substrate was finally diced into 19 × 19 mm² chips, the SU-8 thickness was measured and in some cases it was adjusted by polishing. The device was assembled as illustrated in Fig. 4 and clamped to seal the channel to the transducer board and to assure for correct channel height.

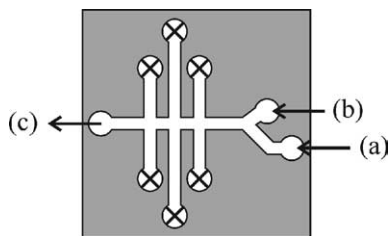


Fig. 3. Channel configuration with inlets for water (a) and particle suspension (b), and a common outlet (c). Excess fluid connections were sealed during evaluation (X).

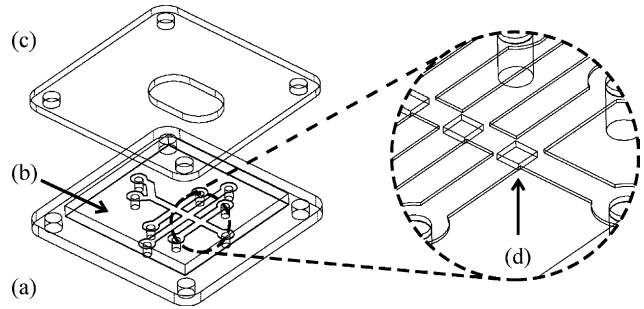


Fig. 4. Assembly of device showing the transducer board (a), supplying fluidic and electrical connections, and the glass/SU-8 microchannel plate (b), which are clamped together using a brass lid (c) with an examination window. In the close-up the position of a transducer element (d) is shown in the channel crossing.

In order to use the soda-lime glass plate (thickness 1.55 mm, sound velocity $v_s = 6000$ m/s [22]) as a $\lambda/4$ reflector, the frequency should be tuned in relation to the plate thickness: 8.7 MHz corresponds to $9\lambda/4$, 10.6 MHz to $11\lambda/4$ and 12.6 MHz to $13\lambda/4$. Between these frequencies the plate has eigenfrequencies corresponding to $(2n + 1)\lambda/2$ at 9.7 MHz and 11.6 MHz. Reflector plates with SU-8 channel heights of 59 μm and 72 μm, corresponding to $\lambda/2$ resonance in water at 12.7 MHz and 10.4 MHz respectively, were chosen for the device assembly. These frequencies do not exactly match the frequencies yielding $\lambda/4$ in the reflector, but was the closest match feasible. The epoxy-covered transducer board and final assembled device are shown in Fig. 5.

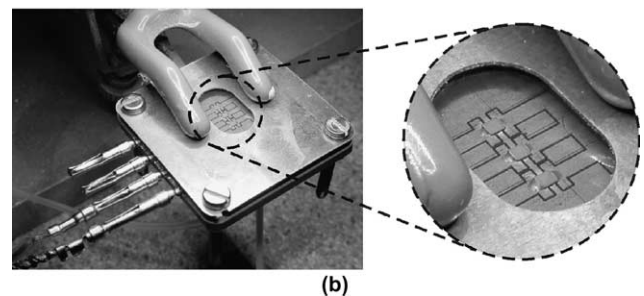
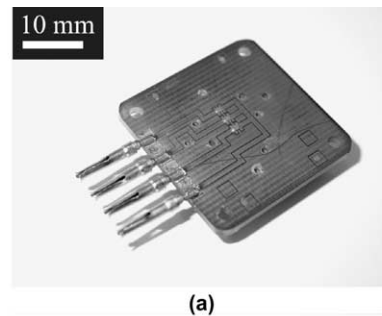


Fig. 5. Finished epoxy-covered transducer board (a) and assembled and connected device for evaluation (b) with a close-up (c) of the examination window.

2.4. Acoustic field distribution

The acoustic field distribution inside the resonator was calculated using the angular spectrum approach (ASA). ASA is based on the fact that if the complex scalar field distribution of a monochromatic wave is Fourier-transformed across any plane the resulting spatial Fourier components can be identified as plane waves travelling in different directions away from that plane [23]. When this plane contains the source field, understood as the field immediately in front of the source, it is designated the source decomposition plane. The field amplitude at any other point in the medium (or across any other parallel plane) can be calculated by adding the contributions of these plane waves, taking into account the phase shifts they have undergone during propagation. ASA enables an efficient analysis of the transmission and reflection from planar interfaces between different media since it formulates scalar diffraction theory in a framework similar to that used in the theory of linear, time invariant systems.

ASA appeared to be a very suitable tool for the analysis of an acoustic field inside the resonator filled with liquid. First, the field emitted by the transducer was expressed as a sum of planar waves with different angles using a two-dimensional fast Fourier transform (2D FFT). As a first approximation it was assumed that the particle velocity vector at the surface was normal to the surface and uniformly distributed, i.e. originating from an ideal piston transducer. Then, the field at the reflector plane was calculated and the wave reflected from the rigid reflector was constructed using principles of geometrical optics. The field inside the resonator was obtained as a superposition of the field emitted by the transducer element and that reflected from the reflector. Thus, two further approximations were made: the second that the internal reflections in the reflector were neglected in the calculations, and the third that the results presented were obtained for one reflection only. Due to the second approximation the resonances resulting from the finite reflector thickness are not modelled. The third approximation was introduced since only approximate pressure patterns were needed for qualitative comparisons with the experiments.

An ASA software package developed for the analysis of elastic fields in solid immersed in water was used for the calculations [24]. First, the distribution of an acoustic field emitted by the transducer element, excited with continuous wave in water (without reflector), was calculated in the parallel and normal planes to the transducer surface. Then, similar calculations were performed for the resonator with the reflector placed at the distance $\lambda/2$ from the transducer.

For measurements of the acoustic field distribution, single transducer elements were mounted on 5 mm diameter round PCBs using similar mounting as de-

scribed above. Measurements were performed using light diffraction tomography with the transducer submerged in water, without the reflector. This technique is an optical measurement method utilizing diffraction of light in a medium with periodical pressure variations due to the propagating ultrasonic wave. The measurement system [25] combines light intensity measurements with tomography algorithms. Compared to hydrophone measurements the method has some important advantages for the applications in this paper. The method is non-perturbing, i.e. no mechanical probe is inserted into the field, making it possible to measure the near field of a miniature ultrasonic transducer. It also offers high-resolution measurements, which is important to be able to resolve the near field pattern of the used transducer elements. The light diffraction tomography system used is schematically pictured in Fig. 6. The transducer was scanned along an axis perpendicular to the laser beam. Once the scan was completed the transducer was returned to its origin, rotated and scanned again. The procedure was repeated until the transducer had been rotated 180° and the results were presented as a pressure map of a plane parallel to the transducer element surface. All measurements in this investigation were performed using 201 samples with a sample distance of 0.01 mm and 50 projections per 180° .

2.5. Device evaluation

The resonant behaviour of mounted transducer elements connected with a coaxial cable was evaluated using a spectrum analyser⁵ equipped with a reflection test kit.⁶ The magnitude and phase angle of the complex impedance were plotted for transducers facing air, as well as for assembled and fluid filled microfluidic devices to obtain information on the system resonances.

To evaluate particle trapping, Teflon tubing connected the inlets of the assembled device to a syringe pump delivering water and to a manually operated syringe delivering particle suspension. The particle suspension⁷ was a blood phantom, mimicking human blood, consisting of 5 μm Orgasol⁸ (polyamide) particles dispersed in water with additional glycerol and dextran. According to the manufacturer the speed of sound in the suspension was 1550 ± 15 m/s. The suspension was diluted with distilled water to a particle volume fraction of 16% as measured from sedimented sample. The device was waterfilled and the excess fluid connections were sealed according to Fig. 3 before injection of particles.

⁵ Agilent 4395A, Agilent, USA.

⁶ Agilent 87512A Transmission/reflection test kit, Agilent, USA.

⁷ EU-DFS-BMF-ver.1, Danish Phantom Service, Denmark.

⁸ Orgasol, Atofina, France.

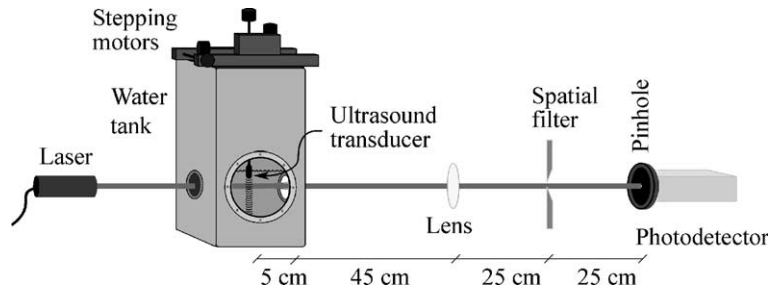


Fig. 6. Experimental set-up of the light diffraction tomography system used for near field acoustic pressure distribution measurements.

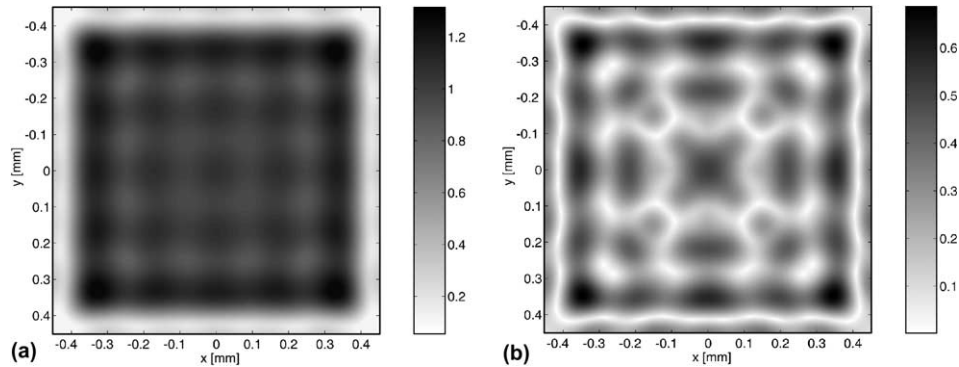


Fig. 7. Calculated acoustic pressure distribution in the water layer above the element surface of a 0.8 mm square piston transducer driven at 10 MHz. The results were calculated for a distance $\lambda/4$ from the transducer surface without (a) and with (b) a reflector positioned $\lambda/2 = 75 \mu\text{m}$ from the transducer surface.

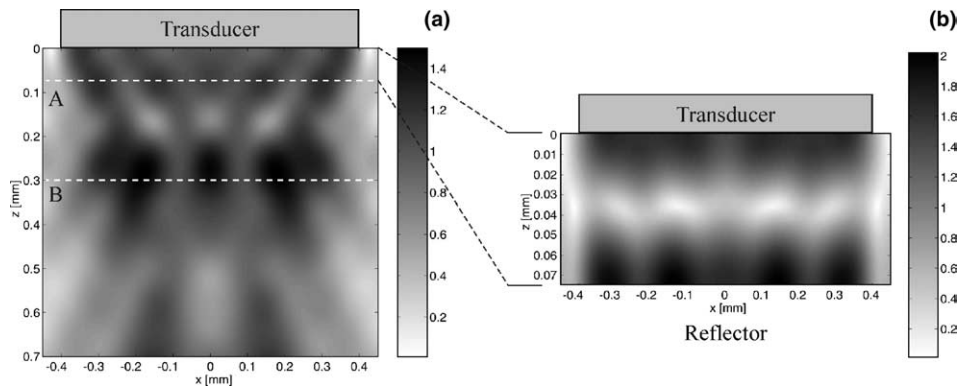


Fig. 8. Calculated acoustic pressure distribution in a plane normal to the surface of a square transducer driven at 10 MHz in water without (a) and with (b) a reflector positioned at $\lambda/2 = 75 \mu\text{m}$ from the transducer surface, indicated by A. The transducer position is at the upper side of the plots and the reflector is situated in the lower side of plot (b). B indicates the plane of calculated pressure distribution in Fig. 9.

The transducer element used for trapping was connected to a function generator⁹ that delivered a 10 V p–p sine voltage signal when connected to a 50 Ω load. Since the impedance of the transducer element varied with frequency, the peak-to-peak voltage over the element was depending on the experimental conditions. Frequencies where the acoustic influences were stronger were qualitatively identified by scanning the frequency

in steps of 100 kHz, from 100 kHz to 15 MHz. The trapping behaviour of particles in the fluid suspension over the transducer element was observed and recorded through the glass examination window of the device using an optical microscope¹⁰ connected to a computerised frame grabber system. The trapping sequence was also recorded using a digital video camera connected

⁹ HP 33120A, Hewlet Packard, USA.

¹⁰ Nikon SMZ 800, Nikon, Japan.

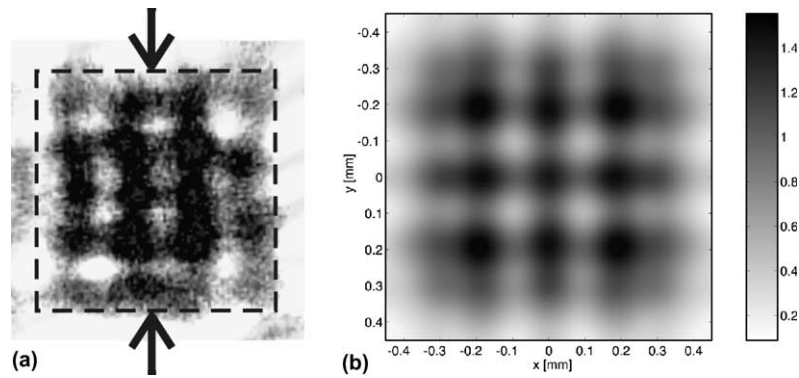


Fig. 9. Measured (a) and calculated (b) pressure distribution at 10 MHz, 0.3 mm from the transducer front surface, corresponding to B in Fig. 8 (a). Dark pixels correspond to high local acoustic pressures. The size and approximate position of the transducer in (a) is outlined together with arrows indicating the sides used for electrical connection.

to the microscope and the trapping speed was evaluated in frame-by-frame playback.

3. Results

3.1. Acoustic field distribution

The calculated acoustic field distributions in a plane parallel to the transducer surface at the distance $\lambda/4$ are shown in Fig. 7(a) and (b). The plots show the pressure distributions for 10 MHz without and with a reflecting surface¹¹ located at the distance $\lambda/2 = 75 \mu\text{m}$ from the transducer surface. The normal particle velocity at the transducer surface was set to 1.0 m/s and the calculated pressure was normalized with the acoustic impedance of water ($1.5 \times 10^6 \text{ kg}/(\text{m}^2\text{s})$). The calculated pressure distributions in a plane normal to the element at its centre without and with reflector are shown in Fig. 8(a) and (b), respectively.

The results from light diffraction tomography measurements performed 0.3 mm (2λ) from the transducer surface at 10 MHz are shown in Fig. 9 together with a calculated pressure distribution in the corresponding plane. Dark pixels in the images indicate high local acoustic pressure.

3.2. Device evaluation

A typical impedance plot of a mounted transducer facing air is shown in Fig. 10. At 10 MHz the impedance is in the order of 10Ω . The resonance spectra of empty respective water filled devices are shown in Fig. 11. The graphs show the magnitude and phase angle of the complex impedance.

¹¹ The glass was assumed to have a density of $2240 \text{ kg}/\text{m}^3$ and longitudinal and transversal wave velocities of 5640 and 3280 m/s, respectively.

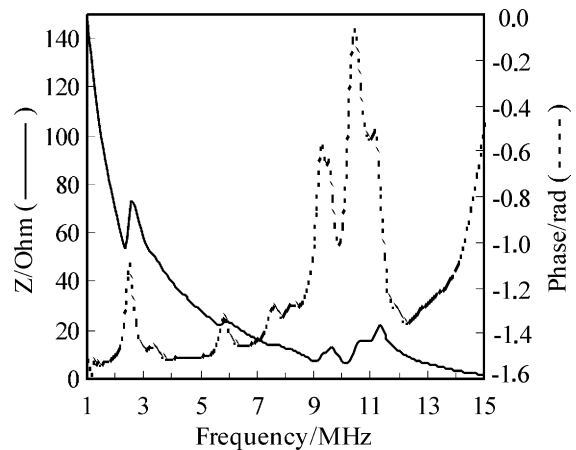


Fig. 10. Plotted impedance magnitude, Z (solid line), and phase (dotted line) of mounted transducer element facing air.

Particle suspension was injected in assembled and water filled devices for the evaluation of particle cluster formation as a function of frequency. During the evaluation there was no externally induced flow in the channel. Fig. 12 shows the trapping area as seen through the examination window for a water-filled device before particle injection. The structure in the particle clusters was studied at operation frequencies from 100 kHz to 15 MHz in steps of 100 kHz. Results received for the $59 \mu\text{m}$ high channel at some frequencies with apparently strong effect on the particle suspension are pictured in Fig. 13. The trapping speed, i.e. the time for the homogeneous particle suspension to fully develop trapped clusters, was estimated to 200 ms by studying individual frames in the captured video sequences (25 frames/s). The slight asymmetry in particle density over the element in e.g. Fig. 13(b) and (c) is due to the existence of a weak flow of particle suspension from the left to the right in the images.

The trapping of particles was evaluated using a channel height of $72 \mu\text{m}$, corresponding to Fig. 11(b) and (d).

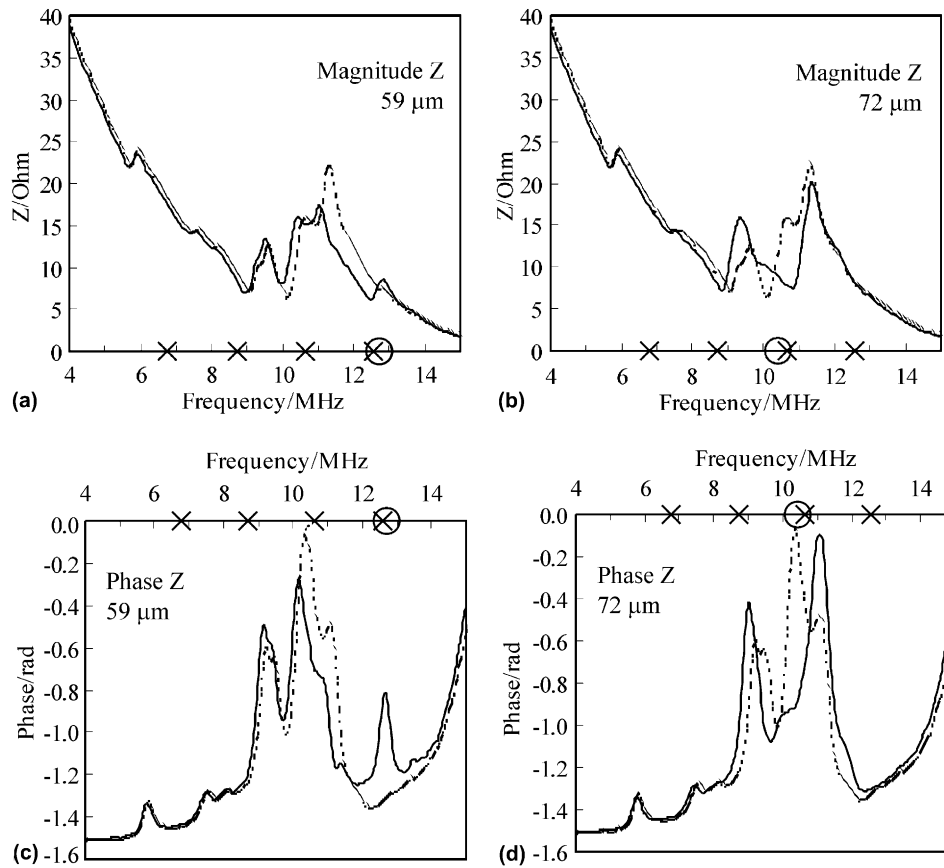


Fig. 11. Magnitude (a–b) and phase (c–d) of impedance for system with empty (dotted line) respectively water filled (solid line) channel of height 59 μm (a and c), respectively 72 μm (b and d). Circles (O) on the frequency axis indicate calculated frequency of $\lambda/2$ in the fluid layer and crosses (X) frequencies corresponding to $(2n+1) \lambda/4$ in the reflector plate.

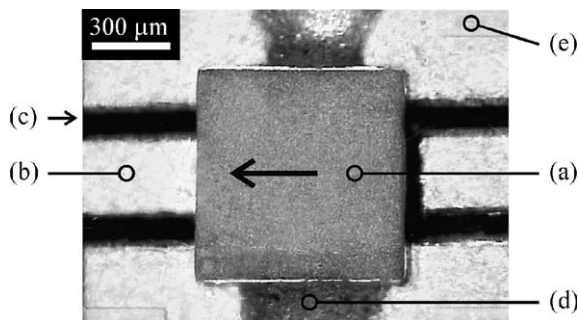


Fig. 12. Particle trapping area, corresponding to Fig. 2, as seen through the examination window showing transducer element (a) mounted using conductive epoxy (d) on PCB with copper layer (b) and milled insulation tracks (c). The pictured element is surrounded by cast and polished epoxy, which covers the copper tracks. The SU-8 (e), forming the 1.0 mm wide channel crossing on the reflector glass plate, can be seen in the corners of the images. An arrow indicates the direction of applied fluid flow.

The evaluation was performed using frequencies near the calculated $\lambda/2$ resonance of the fluid layer, and trapping cycles were captured for frequencies where the effect on particles was found to be strong. A complete

trapping cycle is shown in Fig. 14 for 9.7 MHz, including filling channel with particle suspension, activation of transducer, washing away excessive particles at a flow rate of 4 μl/min and finally release of the trapped particle cluster. The next trapping cycle shown in Fig. 15 was captured at 11.7 MHz using a flow rate of 3 μl/min. At 10.7 MHz, corresponding to the calculated $\lambda/2$ resonance in the fluid layer, the particles were apparently ordered in a plane structure over the transducer but were not trapped at a flow rate of 2 μl/min. The particle cluster formed at this frequency was in correspondence with the result shown in Fig. 13(c), received at 12.5 MHz for the 59 μm channel. Finally, a trapping sequence showing the behaviour upon release when particles are trapped near the interior surfaces of the channel wall is shown in Fig. 16. The sequence is captured for a 90 μm channel at 9.8 MHz.

4. Discussion

Particles passing over the transducer are found to be efficiently trapped by activation of a proper acoustic field. In general, a strong effect on particles is correlated

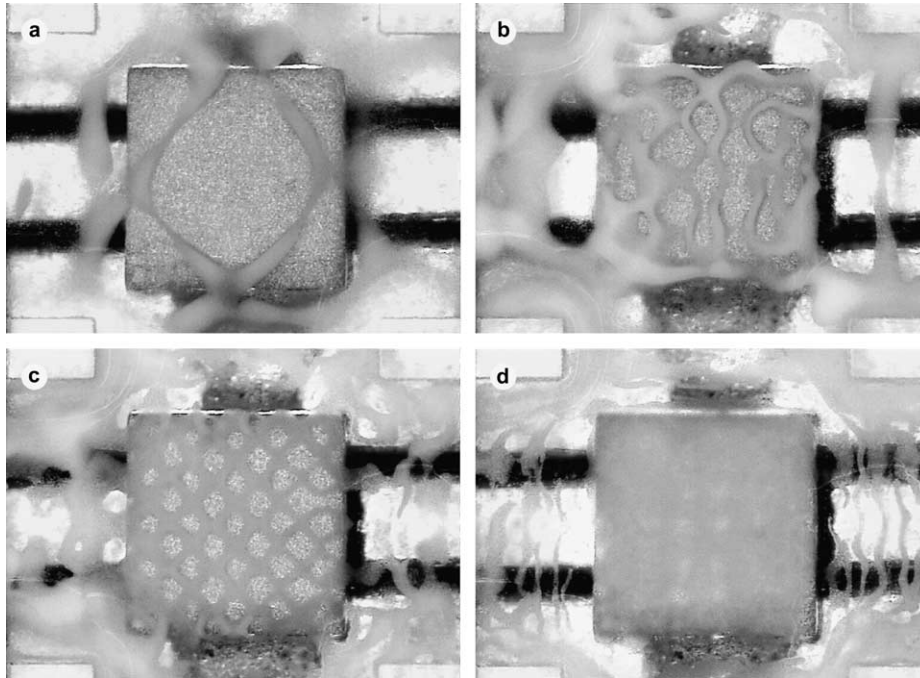


Fig. 13. Particle clusters above transducer element in a 59 μm channel with no externally induced flow captured at: (a) 2.4 MHz; (b) 7.7 MHz, (c) 10.7 MHz and (d) 12.5 MHz.

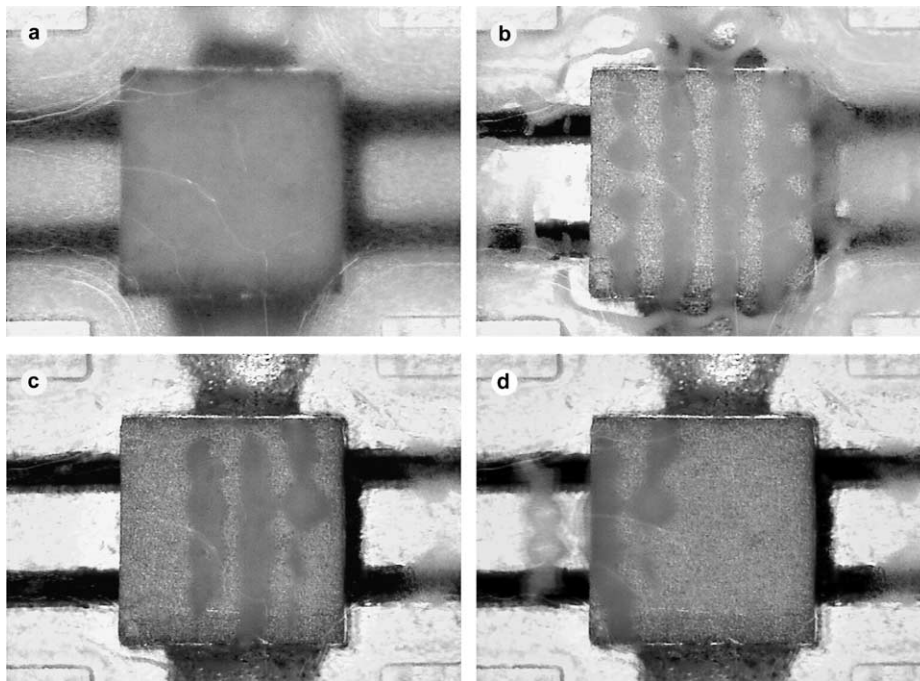


Fig. 14. Trapping cycle over transducer element at 9.7 MHz. The microchannel was filled with particle suspension (a) and the transducer was activated (b). Water was flown at 4 $\mu\text{l}/\text{min}$ from the right to the left in the channel, removing excess particles (c). Particles over the transducer element were held until the transducer was inactivated (d) when they were displaced by the continuous flow to the left.

to the resonances in the device, with the trapping influenced by the transducers acoustical near field. The lateral pressure gradients in the near field help in getting a strong lateral trapping of particle clusters, indicating

that such effects can be utilized in miniaturised systems to increase trapping efficiency.

When subjected to the acoustic field in the vicinity of the transducer the particles form clusters showing a dis-

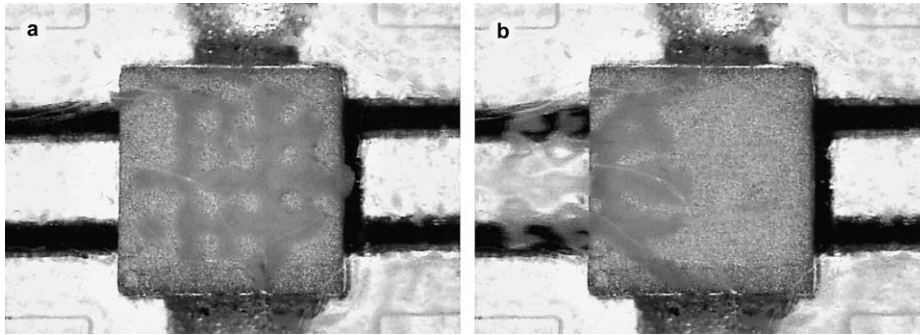


Fig. 15. Trapping cycle over transducer element at 11.7 MHz, (a) and (b) corresponding to (c) and (d) in Fig. 14.

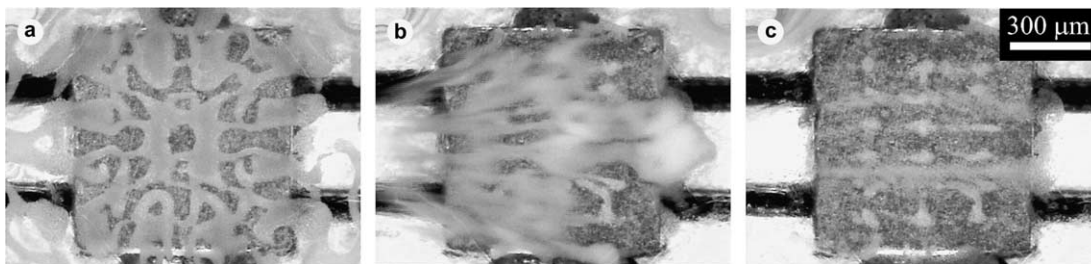


Fig. 16. Trapping cycle over transducer element at 9.8 MHz for a 90 μm channel, (a) and (b) corresponding to (c) and (d) in Fig. 14, leaving particles on the surfaces within the trapping area after release (c). This is an example where particles were trapped near the transducer and/or reflector surfaces.

tinct fine structure as can be seen in Fig. 13. The size, vibration modes and driving frequency of the transducer determine the pressure distribution in the fluid above the transducer surface and therefore also the structure of the trapped particle clusters in the fluid. The near field limit ($d^2/4\lambda$) of a $d = 0.8$ mm diameter circular transducer radiating in water at 10 MHz is approximately 1.1 mm. The acoustic pressure distribution within the near field region is complex, as shown in Fig. 8(a), due to diffraction effects associated with the finite sized transducer element. The calculated near field pressure distribution obtained from the ASA model is shown to agree qualitatively with the structure of the particle clusters. It should be noted that the particles used in the evaluation due to acoustic properties are collected in pressure minima, i.e. in regions between the pressure maxima in Figs. 7 and 8. The results from the light diffraction tomography measurements, Fig. 9(a), are in good agreement with the calculated pressure distribution presented in Fig. 9(b), particularly considering the simplifications associated with the modelled ideal piston transducer. Beside the possibility of different vibration modes in the transducer, deviations between tomography measurements and the calculated results may be explained by individual variations in the transducer elements due to manufacturing and mounting. Some vibration modes with different resonance frequencies are seen in the impedance spectrum of the empty device,

Fig. 11. The resonance near 2.4 MHz is identified as the width resonance of the transducer. The peaks observed at the upper end of the spectrum are interpreted as thickness vibrations incorporating a few smaller peaks that possibly may be explained by the asymmetrical clamping of the element due to mounting. Also the multilayer sandwich electrode design illustrated in Fig. 2 probably influences vibration modes in the transducer, and therefore its acoustical behaviour.

The trapping device was designed to obtain a pressure node located near the middle of the fluid layer by utilizing layered resonator design principles [15] (cf. Fig. 1). The presence of a nodal plane is evident in the calculated pressure distribution, Fig. 8(b), which however does not take into account multiple reflections and transmission in the various interfaces. In the experimental set-up with the 72 μm channel, the channel resonance in the fluid layer was intended to match the thickness resonance of the transducer. As it can be observed near 10.6 MHz in the impedance spectra shown in Fig. 11(b) and (d), the expected resonance at this frequency appear to be moved or split. This is interpreted as an analogy with the two degree of freedom (DOF) vibration absorber effect [16,26]. According to this interpretation a vibrating mechanical system consisting of two coupled parts with coincident individual resonance frequencies demonstrate a splitting of the resonance into two separate resonance peaks surrounding the common

resonance frequency. The splitting of resonances has earlier been observed in ultrasonic spectroscopy analysis of laminate structures with different layers resonating at the same frequency [27]. The measured impedance spectrum of the resonator is complicated, Fig. 11(b) and (d), making it difficult to analyse in detail, but the obtained appearance agrees reasonably well with the 2 DOF vibration absorber effect. Particle trapping using this set-up is stronger at 9.7 and 11.7 MHz as shown in Figs. 14 and 15, possibly due to such a splitting in the system resonance. Another explanation would be that the near-field pattern gets attenuated due to multiple reflections at a frequency corresponding to the resonance in the fluid layer. Further work is needed in order to analyse the behaviour in detail. Trapping and subsequent release of particles was studied to qualitatively evaluate the position of trapped particle clusters in the fluid. If the particle clusters are not kept from the interior surfaces during trapping, particles are still present within the trapping area after release by inactivation of the transducer, as exemplified in Fig. 16. This is an undesirable condition in the future application of the device. In the trapping cycles presented in Figs. 14 and 15 the released cluster leaves no traces of particles. Thus it is concluded that the particles are kept away from the channel walls by the presence of pressure minima between the transducer and the reflector.

The trapping of particle clusters in the device relies on primary transverse radiation forces, which are proportional to the gradient in the acoustic energy density [5]. The results from calculations with the inserted reflector Figs. 7(b) and 8(b) show the existence of periodic lateral pressure gradients in the middle of the channel and in the trapping sequences shown in Figs. 14 and 15 the particles are trapped in a periodic pattern corresponding to the near field pattern. Thus it is concluded that in the evaluated device the periodic variations in the near field pressure constrain the particles laterally. The forces pulling particles together laterally in a standing wave without lateral pressure gradients are weak and originate from scattering of the incident acoustic waves by surrounding particles [5]. The trapping of particle clusters, shown in Fig. 14, is performed at a volumetric flow of 4 $\mu\text{l}/\text{min}$. For a fully developed parabolic flow profile between two parallel plates the local flow rate in the channel centre is 1.5 times higher than the average flow rate as calculated from volumetric flow. In the presented set-up the flow is however widened at the channel crossing over the transducer element with a decrease in average flow rate. It is reasonable to believe that these effects can, as a first approximation, be considered to cancel each other. Thus the volumetric flow of 4 $\mu\text{l}/\text{min}$ used in the trapping experiments then corresponds to a linear flow rate of about 1 mm/s in the centre of the channel above the transducer element, where particles should be trapped. Since neither absolute measurements nor

quantitative simulations of local pressure amplitudes in the resonator were performed, numerical values of the acoustic radiation forces acting on particles could not be calculated. The response speed of the trap, measured as the time to establish a fully developed particle cluster, depends on the strength of forces acting on the particles and the distances needed for the particles to reach a nodal position. Since the distances between nodal positions are small due to both the small dimensions of the microchannel, and to the presence of local pressure minima in the near field of the transducer, the particle trapping is expected to be fast, as proved by the estimated response time of 200 ms.

The particles show some tendency to agglomerate under influence of the ultrasonic field, which can be seen when they move away from the trapping area upon release. This is also evident when supplying a continuous flow of particles; agglomerates of particles can break loose from the trapped cluster. The agglomeration is thought to increase the efficiency of the ultrasonic trapping as compared to single particles since the ultrasonic forces are proportional to the agglomerate volume, while viscous drag increase as a function of the exposed surface area [5]. The acoustically induced influence on particles is not limited to the area directly above the transducer element, but reaches out laterally in the channel, as shown in e.g. Fig. 14(b). However, the forces acting on particles decrease when the distance from the transducer element increases, and particles outside the main trapping area are washed away when applying fluid flow of about 1 $\mu\text{l}/\text{min}$. Thus by introducing miniature transducer elements it is possible to perform highly localized trapping of particle clusters giving way for arrays of individually controllable trapping sites within a microchannel for microbead handling.

5. Conclusions and outlook

Particle clusters consisting of 5 μm polyamide particles were successfully trapped at linear flow rates up to 1 mm/s within a microfluidic channel using acoustic forces. The trapping was performed using miniature PZT multilayer transducer elements integrated in the channel wall, and was making use of ultrasonic standing waves with near field pressure gradients for lateral confinement of the particles. The near field pressure gradients were shown to provide strong lateral trapping, and the particles were kept away from the transducer and reflector surfaces by designing the device to obtain a pressure node near the middle of the channel. The response time of particle trapping was very short; in the order of 200 ms. The integration of miniaturised transducers opens up the possibility to trap particles in an array configuration within a microfluidic chamber, with each trapping site controlled by an individual transducer

element. Microbead handling in such an array format may provide an increase in parallelism and throughput of miniaturised biochemical analysis. Thus, devices for biochemical analysis based on the presented trapping method will be investigated in future work. As a first step a bead-based bioassay will be performed using the fabricated devices. The trapping of beads and their position in the channel will be quantified using fluorescent particles and confocal imaging. Also processing methods that would allow integration and miniaturisation of multilayered transducer elements in two-dimensional arrays will be investigated.

Acknowledgment

The authors would like to thank Dr. Wu Ping at the Department of Engineering Sciences, Uppsala University, for his helpful upgrade of the ASA software. The Swedish Foundation for Strategic Research is acknowledged for its financial support.

References

- [1] H. Andersson et al., Micromachined flow-through filter-chamber for chemical reactions on beads, *Sensors and Actuators B (Chemical)* B67 (1–2) (2000) 203–208.
- [2] R.D. Oleschuk et al., Trapping of bead-based reagents within microfluidic systems: on-chip solid phase extraction and electrochromatography, *Analytical Chemistry* 72 (3) (2000) 585–590.
- [3] S. Ekström et al., On-chip microextraction for proteomic sample preparation of in-gel digests, *Proteomics* 2 (4) (2002) 413–421.
- [4] M. Gröschl, Ultrasonic separation of suspended particles. I. Fundamentals, *Acustica-Acta Acustica* 84 (1998) 432–447.
- [5] S.M. Woodside, B.D. Bowen, J.M. Piret, Measurement of ultrasonic forces for particle–liquid separations, *AIChE Journal* 43 (7) (1997) 1727–1736.
- [6] J. Wu, Acoustical tweezers, *Journal of the Acoustical Society of America* 89 (5) (1991) 2140–2143.
- [7] J.J. Hawkes et al., Single half-wavelength ultrasonic particle filter: predictions of the transfer matrix multilayer resonator model and experimental filtration results, *Journal of the Acoustical Society of America* 111 (3) (2002) 1259–1266.
- [8] A. Nilsson et al., Acoustic control of suspended particles in microfluidic chips. Lab-on-a-chip, Submitted 2003.
- [9] M. Saito, N. Kitamura, M. Terauchi, Ultrasonic manipulation of locomotive microorganisms and evaluation of their activity, *Journal of Applied Physics* 92 (12) (2002) 7581–7586.
- [10] M. Wiklund, S. Nilsson, H.M. Hertz, Ultrasonic trapping in capillaries for trace-amount biomedical analysis, *Journal of Applied Physics* 90 (1) (2001) 421–426.
- [11] M. Wiklund et al., Ultrasonic-trap-enhanced selectivity in capillary electrophoresis, *Ultrasonics* 41 (4) (2003) 329–333.
- [12] A. Nilsson et al., Autologous blood recovery and wash in microfluidic channel arrays utilizing ultrasonic standing waves *MicroTAS 2002*, vol. 2, Kluwer Academic Publishers, Nara, Japan, 2002, pp. 625–626.
- [13] M. Gröschl et al., Ultrasonic separation of suspended particles. III. Application in biotechnology, *Acustica-Acta Acustica* 84 (1998) 815–822.
- [14] M. Gröschl, Ultrasonic separation of suspended particles. II. Design and operation of separation devices, *Acustica-Acta Acustica* 84 (1998) 632–642.
- [15] J. Hawkes et al., Positioning particles within liquids using ultrasound force fields, in: *Proceedings of the Forum Acusticum 2002*, Sevilla, Spain.
- [16] M. Hill, Y. Shen, J.J. Hawkes, Modelling of layered resonators for ultrasonic separation, *Ultrasonics* 40 (1–8) (2002) 385–392.
- [17] R.L. Goldberg, S.W. Smith, Multilayer piezoelectric ceramics for two-dimensional array transducers, *IEEE Transactions on Ultrasonics, Ferroelectrics and Frequency Control* 41 (5) (1994) 761–771.
- [18] G.S. Kino, *Acoustic waves: devices, imaging, and analog signal processing* Prentice-Hall Signal Processing Series, Englewood Cliffs, Prentice-Hall, 1987.
- [19] R.R. Whymark, Acoustic field positioning for containerless processing, *Ultrasonics* (1975) 251–261.
- [20] T. Lilliehorn, U. Simu, S. Johansson, Multilayer telescopic piezoactuator fabricated by a prototyping process based on milling, *Sensors and Actuators A Physical* 107 (2) (2003) 159–168.
- [21] T. Rosqvist, S. Johansson, Soft micromolding and lamination of piezoceramic thick films, *Sensors and Actuators A (Physical)* 97–98 (2002) 512–519.
- [22] J. David, N. Cheeke, Appendix B: acoustic properties of materials, in: *Fundamentals and Applications of Ultrasonic Waves*. 2002, CRC Press LLC.
- [23] J.W. Goodman, *Introduction to Fourier Optics*, 2nd ed., McGraw-Hill, New York, 1996.
- [24] P. Wu, R. Kazys, T. Stepinski, Analysis of the numerically implemented angular spectrum approach based on the evaluation of two-dimensional acoustic fields. Part I and II, *Journal of the Acoustical Society of America* 99 (3) (1996) 1339–1359.
- [25] M. Almqvist et al., High resolution light diffraction tomography—nearfield measurements of 10 MHz CW ultrasound, *Ultrasonics* 37 (1999) 343–353.
- [26] L. Meirovitch, *Fundamentals of vibrations*, McGraw-Hill, New York, 2001.
- [27] J.C. Couchman et al., Resonance splitting in ultrasonic spectroscopy, *IEEE Transactions on Sonics and Ultrasonics* SU-25 (5) (1978) 293–300.